Informatics in Medicine Unlocked 56 (2025) 101650

Contents lists available at ScienceDirect

Informatics in Medicine Unlocked

journal homepage: www.elsevier.com/locate/imu

Enhanced ROI guided deep learning model for Alzheimer's detection using 3D MRI images

Israt Jahan Khan [a], Md. Fahim Bin Amin [a], Md. Delwar Shahadat Deepu [a], Hazera Khatun Hira [a], Asif Mahmud [a], Anas Mashad Chowdhury [a], Salekul Islam [b], Md. Saddam Hossain Mukta [a,c], Swakkhar Shatabda [d,*], and for the Alzheimer's Disease Neuroimaging Initiative [e,1]

[a] Department of Computer Science and Engineering, United International University, Bangladesh
[b] Department of Electrical and Computer Engineering, North South University, Bangladesh
[c] LUT School of Engineering Sciences, Lappeenranta-Lahti University of Technology, Finland
[d] Department of Computer Science and Engineering, BRAC University, Bangladesh
[e] Alzheimer's Disease Neuroimaging Initiative Data Archive, United States of America

ARTICLE INFO

Keywords:
Alzheimer's disease
Regions of Interest (ROIs)
3D MRI
Transfer learning
ResNet 3D
Efficient computation

ABSTRACT

Alzheimer's disease is an incurable condition that predominantly affects the human brain, leading to the shrinkage of various brain regions and the disruption of neuronal connections. Current state-of-the-art methods for detecting Alzheimer's disease using 3D MRI images are resource-intensive and time-consuming. In this paper, we propose a Regions of Interest (ROI)-guided detection paradigm to address these challenges. We employ a 3D ResNet integrated with a Convolutional Block Attention Module (CBAM), demonstrating that emphasising ROIs in brain imaging can substantially reduce both computational expenditure and training time. Our model exhibits robust performance in discriminating Alzheimer's disease from mild cognitive impairment, achieving an accuracy of 88% across the entire brain and 92% within targeted ROIs on the ADNI dataset. The accuracy on the OASIS dataset is even higher, reaching 98% for all regions and 98.33% for the ROIs. When distinguishing Alzheimer's disease from cognitively normal individuals, the accuracy improves further, achieving 93.33% for the ROIs on the ADNI dataset and 97.8% on the OASIS dataset. In differentiating cognitively normal individuals from those with mild cognitive impairment, the model attains an accuracy of 88.2% for the ROIs on the ADNI dataset and 98.6% on the OASIS dataset. These findings highlight a notable enhancement in detection accuracy through the utilisation of fewer, yet more salient brain regions, underscoring the efficacy of our ROI-guided approach.

1. Introduction

The burgeoning field of medical imaging and artificial intelligence (AI) has witnessed remarkable advancements in recent years, transforming the diagnosis and treatment of numerous medical conditions. Among these developments, the analysis of Magnetic Resonance Imaging (MRI) has emerged as an indispensable tool for investigating brain-related disorders, particularly Alzheimer's Disease (AD) [1]. This progressive neurological disorder gradually impairs critical brain regions, leading to a reduction in brain mass. The progression of AD affects multiple areas, including the limbic system, frontal lobe, temporal lobe, parietal lobe, and hippocampus, primarily located within the cerebrum. The cerebrum governs most higher-order functions such as memory, language, and coordination. Currently, no definitive cure exists for Alzheimer's disease, rendering early detection and intervention critical for mitigating its impact and improving the quality of life for affected individuals [2].

According to the Alzheimer's Association, AD progresses through three stages: mild (early), moderate (middle), and severe (late). Traditionally, medical professionals detect these stages by manually analysing MRI images to identify shrinkage in brain regions, particularly within the cerebrum [3,4]. Manual evaluation processes are susceptible to significant human error, potentially resulting in erroneous predictions or misleading assessments. Moreover, conventional detection methods are labour-intensive and inherently subjective, relying

* Corresponding author.
E-mail address: sshatabda@gmail.com (S. Shatabda).

[1] Data used in preparation of this article were obtained from the Alzheimer's Disease Neuroimaging Initiative (ADNI) database (adni.loni.usc.edu). As such, the investigators within the ADNI contributed to the design and implementation of ADNI and/or provided data but did not participate in analysis or writing of this report. A complete listing of ADNI investigators can be found at: https://adni.loni.usc.edu/wp-content/uploads/how_to_apply/ADNI_Acknowledgement_List.pdf.

https://doi.org/10.1016/j.imu.2025.101650
Received 28 September 2024; Received in revised form 3 May 2025; Accepted 4 May 2025
Available online 22 May 2025
2352-9148/© 2025 Published by Elsevier Ltd. This is an open access article under the CC BY-NC-ND license (http://creativecommons.org/licenses/by-nc-nd/4.0/).

heavily on the expertise and judgement of medical professionals, which may vary [5]. By contrast, deep learning offers a more effective and precise alternative by autonomously analysing MRI scans, reducing human error, processing large volumes of data swiftly, and detecting nuanced patterns that facilitate earlier and more accurate diagnoses. The integration of AI into clinical workflows enhances diagnostic accuracy and supports the development of personalised treatment plans, thereby improving patient outcomes [5,6].

Recent progress in machine learning and deep learning has paved the way for innovative diagnostic strategies for AD. Inan et al. [7] and Arya et al. [8] conducted comprehensive reviews of machine learning and deep learning methods for AD, focusing on sMRI and PET imaging data from the ADNI and OASIS datasets. Biswas et al. [9] developed a system for early diagnosis by classifying disease severity using machine learning algorithms. Ayus et al. [10] introduced ALZ-IS, an automated Alzheimer's identification system based on HReENet, and Lei et al. [11] proposed a hybrid federated learning approach with a Brain-region Attention Network.

El-Assy et al. [12] designed a dual CNN-based framework for early detection, while Balasundaram et al. [1] employed a multilayered CNN and ResNet50 to target the hippocampus region. Helaly et al. [13] presented the DL-AHS framework for hippocampus segmentation and AD detection. Furthermore, Carcagni et al. [14] incorporated a vision transformer with CNNs for sMRI images, and Sang et al. [15] utilised a graph convolutional neural network for AD classification.

Several other studies have pursued multimodal approaches. Wang et al. [16] predicted AD progression from MCI using multimodal data integration, while Yaqoob et al. [17] proposed a ResNet-self architecture with a fuzzy entropy-controlled path-finding algorithm. These studies collectively underscore the diversity and innovation characterising the advancement of Alzheimer's Disease diagnosis through sophisticated machine learning and deep learning techniques.

Nevertheless, models utilising 3D MRI images [1,7–9,13,14,17–19] face substantial computational challenges. Training with 3D MRI data demands significant resources in terms of computational power and memory [20,21]. The complexity of 3D models necessitates sophisticated preprocessing tools and extended training durations, rendering these models cost-prohibitive and less feasible for widespread deployment. In contrast, 2D MRI-based models are comparatively less demanding computationally and faster to train [10,11,16,22–25]. However, reliance on 2D slices may result in the loss of critical spatial information inherent in 3D data, potentially diminishing diagnostic accuracy and the ability to detect subtle volumetric changes crucial for early AD diagnosis [7].

Rangaraju et al. [26] proposed a 3D MRI-based Dual Attention Aware Depth-Wise Separable Convolution (DA-DSC) network, achieving 99.87% test accuracy on the ADNI dataset. Ramya et al. [27] introduced a framework combining 2D Adaptive Bilateral Filtering, ECLAHE image enhancement, and ROI segmentation, achieving 96.92% accuracy using Logistic Regression classifiers.

Moreover, Odusami et al. [28] developed an early feature fusion framework by integrating MRI and PET images, enhancing classification through a modified ResNet18 architecture. Further, Odusami et al. [29] fused sMRI and FDG-PET data using a static pulse-coupled neural network with a Laplacian pyramid, employing a Mobile Vision Transformer (MViT) optimised by Pareto-Optimal Quantum Dynamic Optimisation to classify AD stages, demonstrating high precision and sensitivity.

The present research addresses key limitations identified in the existing literature on Alzheimer's Disease detection. Despite noteworthy progress, current state-of-the-art methods remain computationally intensive and time-consuming, thereby limiting real-world applicability. Furthermore, many approaches require manual intervention, decreasing feasibility for deployment.

In this study, a computationally efficient and fully automated model is proposed for Alzheimer's Disease detection using 3D MRI images. Unlike most studies relying on entire brain scans [7,8], the proposed method focuses on Region of Interest (ROI)-based analysis to significantly reduce training time without compromising performance [11,14,16].

A unified pipeline is developed, autonomously executing preprocessing using FastSurfer-processed 3D images, followed by training and prediction phases, eliminating the need for manual intervention. This end-to-end automation enhances reproducibility and reliability of experimental outcomes.

A GitHub repository containing the full codebase has been provided to validate the reproducibility of the results. Additionally, attention mechanisms are incorporated within the CNN architecture to prioritise salient features and suppress irrelevant background noise, thereby improving model discriminative capability and overall diagnostic performance [12,22,30].

In this study, a 3D ResNet integrated with a Convolutional Block Attention Module is employed. FastSurfer is utilised for MRI preprocessing to achieve accurate and efficient skull stripping. By processing 3D MRI data directly, the need for 2D conversion is eliminated. Performance comparisons are conducted using two settings: processing all brain regions and focusing only on the six most affected regions (ROIs). This approach demonstrates reduced runtime and enhanced classification accuracy on two benchmark datasets, ADNI and OASIS, for discriminating Alzheimer's Disease from mild cognitive impairment and cognitively normal subjects.

The novelty of our work lies in emphasising specific Regions of Interest (ROIs) within 3D MRI brain scans. This ROI-based methodology optimises computational resource utilisation and minimises training time while achieving robust and accurate detection outcomes. Transformer-based architectures, such as Vision Transformers (ViTs), were deliberately avoided due to their substantial computational demands and the necessity for extensive datasets to achieve optimal performance. Instead, a ResNet18 integrated with a Convolutional Block Attention Module (CBAM) was employed, providing an effective balance between computational efficiency and predictive capability, and aligning well with the constraints and scope of our dataset.

2. Materials and methods

In this section, we provide an overview of our proposed method, including dataset collection, preprocessing, ROI selection, augmentation, registration, and model selection. A schematic diagram is shown in Fig. 1. The process begins with data collection, where 3D image data are obtained from the ADNI (ADNI 1.5T Screening) and OASIS (OASIS1) datasets. After data collection, we segment the 3D MRI images. Using the FastSurfer tool, we perform skull stripping and segmentation.

For model training and testing, we divide the dataset into an 80/20 split (80% for training and 20% for testing). To improve image contrast while preserving details, we apply CLAHE (Contrast Limited Adaptive Histogram Equalisation) during image loading [31]. Subsequently, image sharpening is applied to enhance image quality.

To ensure consistency across samples, MRI registration is performed by aligning a moving image with a fixed image through a non-linear registration process. To enhance the model's robustness, we apply rotation-based data augmentation techniques, introducing variations into the dataset.

We consider the 3D ResNet model as our base architecture. Additionally, we extend the 3D ResNet by integrating an attention mechanism called CBAM (Convolutional Block Attention Module). CBAM is a powerful attention mechanism designed to enhance the representational power of CNNs by capturing channel-wise and spatial-wise dependencies in feature maps [32,33]. By adaptively attending to relevant features, CBAM improves both the performance and interpretability of CNN and neural network-based 3D models across various computer vision tasks [32].

Finally, we conduct evaluation procedures to assess the model's performance across all brain regions and specific regions of interest (ROIs), ensuring accurate and efficient disease prediction with reduced runtime.

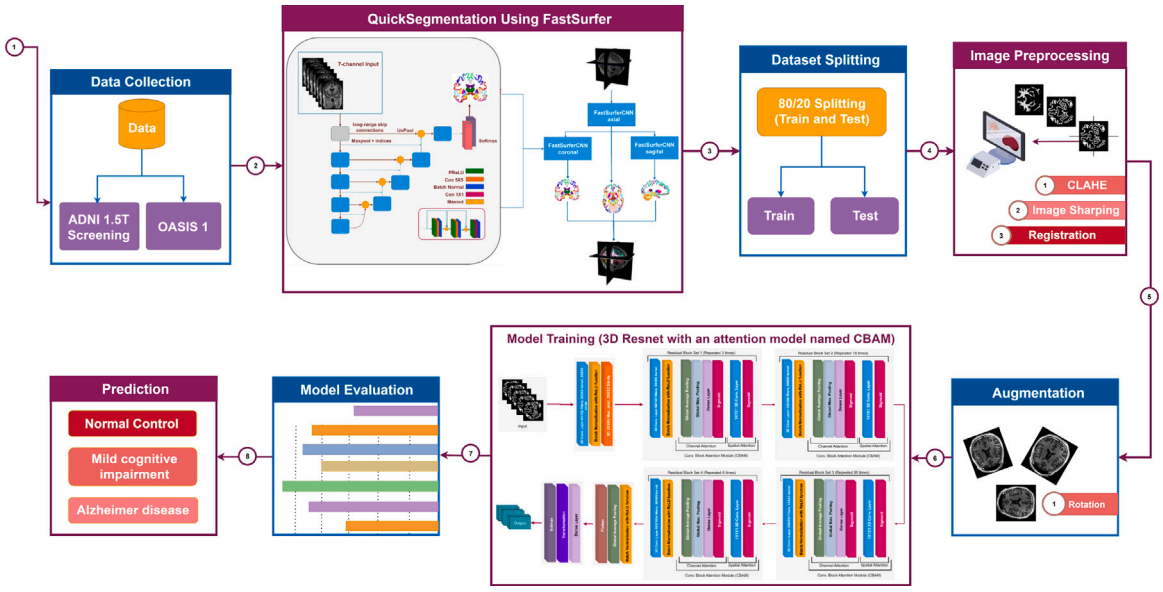


Fig. 1. Overall pipeline for detection of Alzheimer's disease from 3D MRI.

2.1. Datasets

We use MRI images from two sources: the Alzheimer's Disease Neuroimaging Initiative (ADNI) and the Open Access Series of Imaging Studies (OASIS).

ADNI dataset

We utilise structural magnetic resonance imaging (sMRI) data that is T1-weighted and acquired at a field strength of 1.5 T (1.5T) [18]. The dataset includes individuals who underwent screening and received scans at 6 and 12 months. For this study, we select the original scan for each participant prior to the initiation of any medication or treatment. These baseline scans provide consistent data for our investigation.

Within the ADNI dataset, participants are categorised into three diagnostic groups: Mild Cognitive Impairment (MCI), Alzheimer's Disease (AD), and Cognitively Normal (CN). The Alzheimer's Disease (AD) group includes 133 subjects aged between 68 and 83 years, with a gender distribution of 69 males and 64 females. The Mild Cognitive Impairment (MCI) group comprises 316 subjects, also aged between 68 and 83 years, with 206 males and 110 females. The Cognitively Normal (CN) group consists of 196 subjects aged from 71 to 82 years, with 103 males and 93 females.

OASIS dataset

The OASIS dataset includes preprocessed MRI images from 1688 subjects, ranging in age from 18 to 96 years. Three or four separate T1-weighted MRI scans were performed for each individual during a single scanning session. The cohort comprises both male and female subjects, all of whom are right-handed [34]. The data originates from the Open Access Series of Imaging Studies (OASIS-1). Regarding subject distribution, the AD group comprises 117 subjects with Clinical Dementia Rating (CDR) values of 1.0 and 2.0. The CN group consists of 1301 subjects with a CDR value of 0.0, indicating no cognitive impairment. The MCI group includes 270 subjects with a CDR value of 0.5, representing mild cognitive impairment.

2.2. 3D MRI preprocessing

In this step, traditional preprocessing methods are applied to enhance the clarity and quality of the MRI images. Skull stripping is performed to remove non-brain regions, followed by the application of CLAHE (Contrast Limited Adaptive Histogram Equalisation) to improve image contrast. Image sharpening is employed to further enhance detail, and MRI registration is conducted to align the images. Additionally, data augmentation techniques are applied to increase dataset variability and improve model robustness (see Fig. 2).

The entire image dataset was divided into two parts after applying FastSurfer QuickSeg to extract the brain regions. The split was performed in an 80/20 ratio, with 20% allocated for testing and 80% for training. This procedure was applied separately to both the ADNI and OASIS datasets. Additionally, the dataset was balanced by oversampling the minority class prior to splitting in order to prevent the model from being biased towards the dominant class.

2.2.1. Skull stripping

FastSurfer QuickSeg [35], a deep learning architecture, was used for skull stripping to extract the brain from raw MRI images, improving brain analysis by removing non-brain tissues. A visual example of the skull-stripped MRI is shown in Fig. 3. The entire research workflow and experiments are fully reproducible, and the complete codebase has been open-sourced. The code is available on GitHub.[2]

2.2.2. Region of interest selection

After extracting the brain using FastSurfer QuickSeg (Quick Segmentation), specific regions of interest (ROIs) were selected by removing non-relevant brain areas. Six ROIs significantly affected by Alzheimer's Disease progression were identified: the left and right cerebral white matter, the left and right cerebellum white matter, and the left and right hippocampus. Only these ROIs were retained, while other brain regions were removed.

The selection of these six ROIs was based on findings from prior research in Alzheimer's Disease (AD) detection. These regions are known to play critical roles in AD progression. The cerebral white matter is often affected early in AD, exhibiting significant atrophy and disruption of neural pathways, making it crucial for early detection [36]. Although less studied, the cerebellar white matter has also been associated with cognitive decline in AD, with emerging research highlighting its importance. The hippocampus is widely recognised for its pronounced volume loss in AD, which strongly correlates with cognitive deterioration. By focusing on these specific regions, the proposed approach captures early signs of the disease that may not be as apparent across the entire brain, thereby improving model sensitivity and accuracy.

[2] GitHub: https://github.com/FahimFBA/Alz-Predict-ROIvsNonROI/.

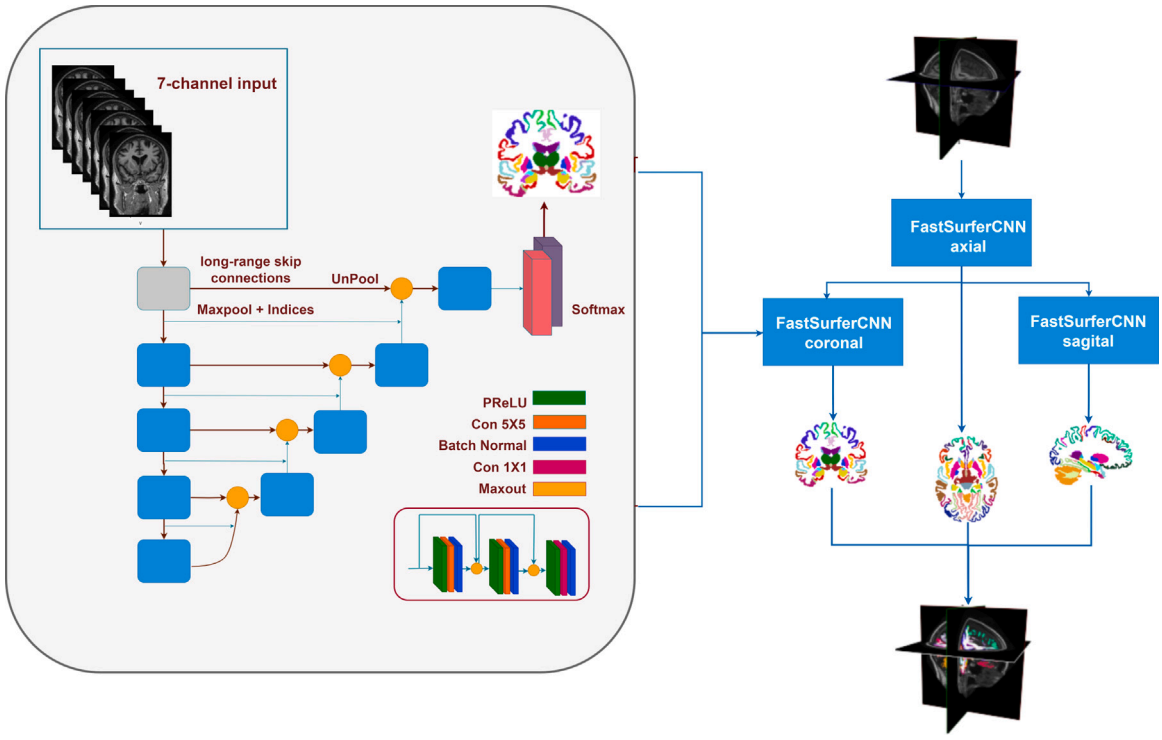


Fig. 2. Visual illustration of FastSurfer QuickSeg.

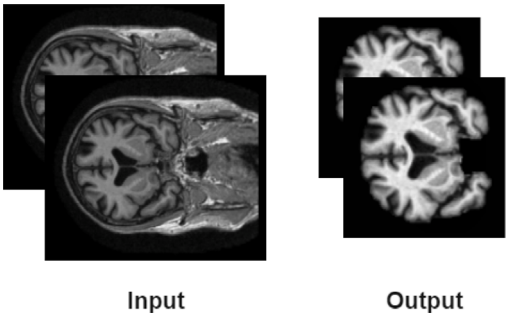


Fig. 3. Visual illustration of skull stripping.

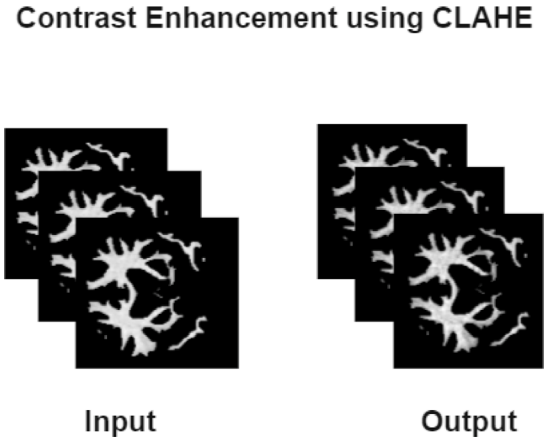


Fig. 4. Visual illustration of CLAHE.

2.2.3. Histogram equalisation

To improve image contrast while preserving details, CLAHE (Contrast Limited Adaptive Histogram Equalisation) was applied during the image loading process. CLAHE, a variation of the Adaptive Histogram Equaliser [37], mitigates the over-amplification of contrast. Instead of being applied to the entire image, CLAHE operates on discrete small regions known as tiles. Bilinear interpolation is subsequently used to combine neighbouring tiles and eliminate artificial boundaries. A visual illustration of the CLAHE application is shown in Fig. 4.

Without CLAHE, the images exhibit poor contrast and diminished detail, as shown on the input side of Fig. 4. CLAHE enhances both contrast and detail, as illustrated on the output side of the same figure.

We have several 2D slices stacked along a specific dimension to create a 3D MRI image. The clip limit is set to 2.0, controlling the degree of contrast enhancement, where a higher value results in greater contrast. The tile grid size is defined as 8 × 8, denoting the size of the contextual regions (tiles) used for histogram equalisation. Each 2D slice is divided into non-overlapping tiles. The histograms are then clipped and equalised for each tile. After processing each tile, bilinear interpolation is used to smooth transitions between adjacent tiles, and the processed tiles are combined back into the full 2D slice. The above steps are applied sequentially to each 2D slice within the 3D MRI volume.

2.2.4. Image sharpening

Unsharp masking [38] was used to enhance the sharpness of the images. Unsharp masking is a linear image processing technique that sharpens an image by amplifying high-frequency components. Image sharpening enhances the edges and fine details, making the images clearer and improving overall image quality.

$$\text{enhanced_image} = \text{original} + \text{amount} \times (\text{original} - \text{blurred})$$

2.2.5. Augmentation and registration

After preprocessing steps, data augmentation was performed using random rotation. This random rotation introduced variations in the training images, followed by a symmetric diffeomorphic registration

approach, which was utilised to ensure accurate alignment between images.

The method involved rotating images by random angles selected within a specified range. The angle was chosen randomly between a negative and positive range, allowing clockwise or counterclockwise rotations. This rotation alters the orientation but preserves the size and shape of the image. Random rotation enables the model to learn from different perspectives, simulating real-world variations in MRI acquisition.

No hyperparameter tuning was applied in this research. Key settings such as learning rate, batch size, number of epochs, number of filters in convolutional layers, and dropout rate were fixed. Specifically, the learning rate was set to 0.001, the batch size to 32, the dropout rate to 0.2, and L2 regularisation with a strength of 0.01 was used. The Adam optimiser was employed with a learning rate of 0.001.

Random rotation as part of data augmentation improved the model's adaptability to different image orientations. In practical scenarios, MRI images may be acquired at varying angles; random rotation helps the model generalise better to such variations. Including random rotation during training enables the model to learn orientation-invariant features, enhancing its robustness to new, unseen data while adding minimal computational cost.

The impact of data augmentation, including random rotation, on model performance was evaluated. Models trained with augmentation demonstrated improved accuracy, better feature recognition, and reduced overfitting on unseen datasets.

Registration is another crucial preprocessing step, where all MRI images are aligned to a common anatomical space. This ensures consistent analysis across samples, even if images were acquired at different positions or angles. Accurate alignment enhances the model's ability to learn relevant features.

The influence of registration errors on model performance was also assessed. It was observed that minor registration inaccuracies did not significantly impact classification accuracy, indicating the robustness of the proposed method.

2.3. 3D ResNet model architecture

The 3D model starts with an input layer, followed by a 3D convolutional layer with 64 filters for Regions of Interest (ROIs) and 128 filters for all brain regions. This layer captures spatial features from the input volume using a $5 \times 5 \times 5$ kernel and a stride of $2 \times 2 \times 2$. Batch normalisation and a ReLU activation function follow this layer to stabilise training and introduce non-linearity. A 3D max pooling layer with a $3 \times 3 \times 3$ pool size and a $2 \times 2 \times 2$ stride is then applied to reduce spatial dimensions and control overfitting through down-sampling.

The network proceeds through four sets of residual blocks, each containing multiple residual blocks. The first set consists of three residual blocks, each with a 3D convolutional layer (64 filters for ROIs, 128 for all brain regions) using a $5 \times 5 \times 5$ kernel, followed by batch normalisation and ReLU activation. This is repeated for another 3D convolutional layer with the same configuration. A Convolutional Block Attention Module (CBAM) is then applied, enhancing feature representation through channel attention (using global average pooling, global max pooling, dense layers, and sigmoid activation) and spatial attention (using 3D convolution and sigmoid activation).

The second set of residual blocks contains sixteen blocks, each with 3D convolutional layers with 128 or 256 filters. The third set includes thirty-six blocks with 256 or 512 filters. The fourth set comprises six blocks with 512 or 1024 filters. Each set follows the same CBAM configuration and connection pattern.

After these residual block sets, batch normalisation and ReLU activation functions are applied to the resulting feature maps. Spatial dimensions are reduced through global average pooling, which computes the average value of each feature map. This pooled output is flattened into a single vector. Finally, a dense (fully connected) layer with units equal to the number of output classes produces the final predictions. Depending on the task, a softmax activation function is applied for binary classification, resulting in predicted class probabilities or scores. The model architecture is given in Fig. 5.

2.4. Details of model architecture

Our model is based on a 3D ResNet with a Convolutional Block Attention Module (CBAM) to detect Alzheimer's Disease (AD) using MRI scans. The design focuses on both spatial and channel-wise features, with special attention to brain Regions of Interest (ROIs).

The model begins with an input layer followed by a 3D convolutional layer, utilising 64 filters for ROIs and 128 filters for other brain regions. These filter numbers were selected to effectively capture detailed patterns while maintaining computational efficiency. The kernel size is set to $5 \times 5 \times 5$, allowing the model to capture both fine and coarse features within the 3D MRI scans. This kernel size enables the identification of critical brain structures associated with AD while keeping the network lightweight and less resource-intensive.

To reduce feature map dimensions while preserving essential spatial information, a stride of $2 \times 2 \times 2$ and a pooling size of $3 \times 3 \times 3$ are used. Residual blocks are incorporated to facilitate training and mitigate degradation issues in deep networks. The model architecture begins with 64 and 128 filters to capture low-level features and progressively increases to 256, 512, and 1024 filters to extract higher-level, more complex patterns. Increasing the number of filters allows the model to learn subtle differences as it progresses deeper into the network.

The Convolutional Block Attention Module (CBAM) helps the model focus on the most important features in the data. CBAM applies channel attention to prioritise the most informative channels, enhancing features strongly correlated with AD. It also applies spatial attention to emphasise specific brain regions within the MRI scans, particularly those most affected by AD.

Following feature extraction through residual blocks and CBAM, global average pooling is applied to reduce the spatial dimensions and summarise the learned features. The resulting feature vector is then passed through a dense (fully connected) layer to perform the final classification, predicting the presence or absence of AD.

CBAM proves particularly effective for AD detection by ensuring the model focuses on the most critical areas and features indicative of the disease. As changes associated with AD are often subtle and localised, CBAM enhances the model's capability to detect these minor variations, improving overall diagnostic accuracy. The proposed model is thus designed to efficiently and accurately detect AD, even when the pathological changes in the brain are difficult to observe.

2.5. Evaluation metrics

Several evaluation metrics were employed to assess the performance of the model, including accuracy score, confusion matrix, precision score, recall score, area under the curve (AUC), and F1 score.

- **Accuracy score:** The accuracy score is one of the most widely used metrics in machine learning and deep learning. It expresses the proportion of accurately predicted instances (True Positives and True Negatives) relative to the total instances (True Positives, True Negatives, False Positives, and False Negatives). It provides an overall measure of the model's prediction correctness.

$$\text{Accuracy} = \frac{\text{Number of Correct Predictions}}{\text{Total Number of Predictions}}$$

- **Precision:** Precision assesses the accuracy of positive predictions (True Positives). It measures the ratio of correctly predicted positive instances to the total predicted positives (True Positives and False Positives). Thus, it provides insight into the reliability of the model's positive classifications.

$$\text{Precision} = \frac{\text{True Positives}}{\text{True Positives} + \text{False Positives}}$$

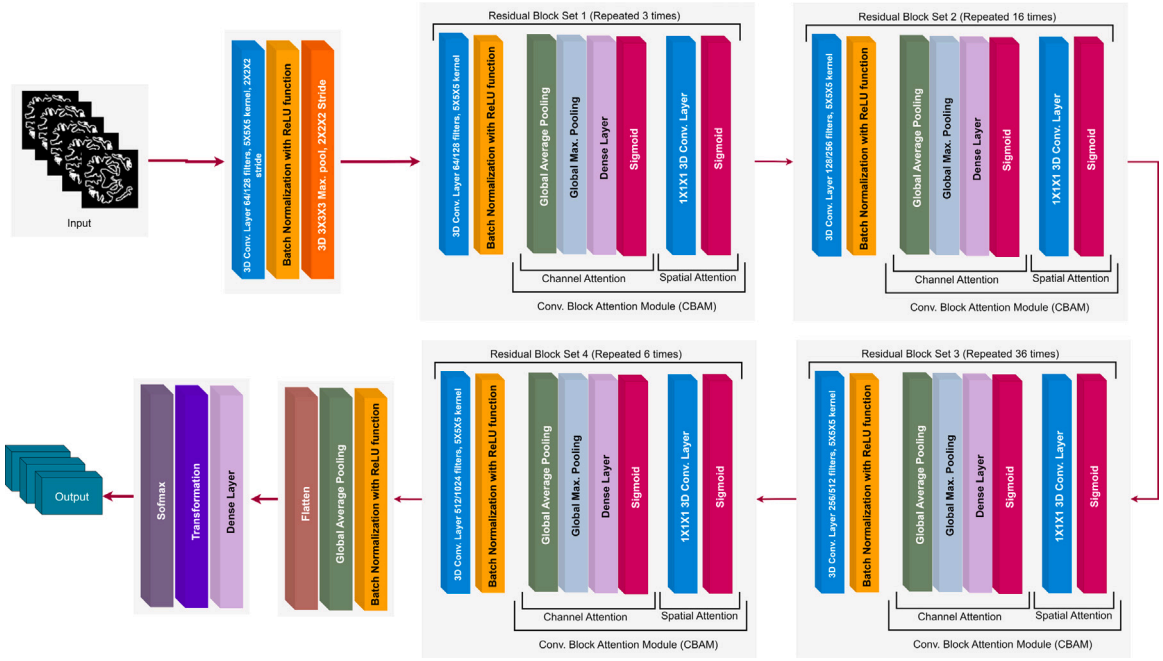


Fig. 5. Visual illustration of 3D-ResNet architecture.

- **Recall:** Recall represents the ability of the model to capture all relevant instances by calculating the ratio of True Positive predictions to the total actual positives.

$$\text{Recall} = \frac{\text{True Positives}}{\text{True Positives} + \text{False Negatives}}$$

- **F1 score:** The F1 score combines precision and recall using their harmonic mean and provides a balanced evaluation metric. It is particularly suitable for assessing model performance in scenarios involving imbalanced class distributions.

$$\text{F1 Score} = 2 \times \frac{\text{Precision} \times \text{Recall}}{\text{Precision} + \text{Recall}}$$

- **AUC-ROC score:** The Area Under the Receiver Operating Characteristic Curve (AUC-ROC) score evaluates how well a binary classification model can distinguish between two classes, such as positive and negative samples. The ROC curve plots the true positive rate (how often the model correctly predicts positives) against the false positive rate (how often the model incorrectly predicts negatives as positives) at various threshold settings.
  The AUC score represents the area under the ROC curve and ranges from 0 to 1. Here, 1 indicates that the model correctly identifies all positive and negative cases, 0.5 suggests the model is no better than random guessing, and 0 implies completely incorrect predictions.

$$\text{AUC} = \int_0^1 \text{TPR}(\text{FPR})\, d(\text{FPR})$$

These evaluation metrics provide a comprehensive assessment of the model's accuracy, precision, recall, discrimination ability, and overall performance, offering valuable insights into its effectiveness for binary classification tasks.

3. Experimental analysis

In this section, the performance evaluation and analysis of the proposed model are presented. The system specifications used for the experiments are as follows: the operating system was Ubuntu 16.04.1, with an Intel(R) Core(TM) i7-7700 CPU running at 3.60 GHz. For graphics processing, the system utilises an NVIDIA TITAN Xp GPU with 12 GB of VRAM. Additionally, the system is equipped with 32 GB of RAM.

Table 1
Experimental results on two datasets for AD vs MCI.

Experiment	Accuracy	Recall	AUC	Precision
ADNI (All Regions)	88%	88%	93%	83.33%
ADNI (6 ROIs)	92%	91.67%	94%	92%
OASIS (All Regions)	98%	97.7%	99.55%	98%
OASIS (6 ROIs)	98.33%	98%	99.8%	98.33%

3.1. Results

This section provides an overview of the performance evaluation of the model across three distinct binary classification tasks: Alzheimer's Disease (AD) versus Mild Cognitive Impairment (MCI), Cognitively Normal (CN) versus Alzheimer's Disease (AD), and Cognitively Normal (CN) versus Mild Cognitive Impairment (MCI).

Alzheimer's disease (AD) vs. Mild cognitive impairment (MCI)

The results for the AD vs. MCI classification task are summarised in Table 1. For the ADNI dataset using all brain regions, the model achieved an accuracy of 88%, a recall of 88%, an AUC of 93%, and a precision of 83.33%. When focusing on the six selected Regions of Interest (ROIs), the performance improved, achieving an accuracy of 92%, a recall of 91.67%, an AUC of 94%, and a precision of 92%.

For the OASIS dataset using all brain regions, the model achieved an accuracy of 98%, a recall of 97.7%, an AUC of 99.55%, and a precision of 98%. When focusing on the six ROIs, the performance slightly improved further, reaching an accuracy of 98.33%, a recall of 98%, an AUC of 99.8%, and a precision of 98.33%.

These results highlight the effectiveness of focusing on specific brain regions impacted by Alzheimer's Disease, especially when advanced preprocessing and segmentation techniques are applied. The consistent improvements observed using the six ROIs suggest that targeted analysis can yield more accurate and reliable predictions in the AD vs. MCI classification task.

Table 2
Experimental results on two datasets for CN vs AD.

Experiment	Accuracy	Recall	AUC	Precision
ADNI (All Regions)	88.89%	89%	93.5%	89.33%
ADNI (6 ROIs)	93.33%	93%	94%	92%
OASIS (All Regions)	95%	95%	99.38%	96.2%
OASIS (6 ROIs)	97.8%	98%	99.6%	97.5%

Table 3
Experimental results on two datasets for CN vs MCI.

Experiment	Accuracy	Recall	AUC	Precision
ADNI (All Regions)	87.27%	87%	88.5%	88.21%
ADNI (6 ROIs)	88.2%	88%	91.12%	89%
OASIS (All Regions)	98.05%	98%	99.5%	98%
OASIS (6 ROIs)	98.6%	98.6%	99.85%	98%

Table 4
Training time for each epoch (in seconds).

Experiment	ADNI		OASIS	
	All regions	6 ROIs	All regions	6 ROIs
AD vs MCI	500 to 520	470 to 480	1700 to 1900	1362 to 1500
AD vs CN	345 to 366	330 to 350	1500 to 1660	1150 to 1350
CN vs MCI	430 to 450	423 to 450	1700 to 1850	1350 to 1400

Cognitively normal (CN) vs. Alzheimer's disease (AD)

The performance metrics for the CN versus AD classification task are summarised in Table 2. Experiments were conducted using both the ADNI and OASIS datasets, comparing the use of all brain regions versus six selected ROIs.

For the ADNI dataset using all brain regions, the model achieved an accuracy of 88.89%, a recall of 89%, an AUC of 93.5%, and a precision of 89.33%. When utilising the six ROIs, the accuracy improved to 93.33%, with a recall of 93%, an AUC of 94%, and a precision of 92%.

For the OASIS dataset, using all brain regions, the model achieved an accuracy of 95%, a recall of 95%, an AUC of 99.38%, and a precision of 96.2%. When focusing on the six ROIs, further improvements were observed, with an accuracy of 97.8%, a recall of 98%, an AUC of 99.6%, and a precision of 97.5%.

Cognitively normal (CN) vs. Mild cognitive impairment (MCI)

The performance metrics for the CN versus MCI classification task are detailed in Table 3. Experiments were performed using both the ADNI and OASIS datasets, comparing performance with all brain regions versus six selected ROIs.

For the ADNI dataset using all brain regions, the model achieved an accuracy of 87.27%, a recall of 87%, an AUC of 88.5%, and a precision of 88.21%. When focusing on the six ROIs, slight improvements were observed, with an accuracy of 88.2%, a recall of 88%, an AUC of 91.12%, and a precision of 89%.

For the OASIS dataset, the model achieved an accuracy of 98.05%, a recall of 98%, an AUC of 99.5%, and a precision of 98% when using all brain regions. When utilising the six ROIs, the model further improved, achieving an accuracy of 98.6%, a recall of 98.6%, an AUC of 99.85%, and a precision of 98%.

These results suggest that focusing on specific brain regions affected by cognitive impairment enhances model performance, as reflected by improvements in accuracy, recall, AUC, and precision, consistent across all three binary classification tasks.

3.2. Model complexity analysis

Table 4 summarises the training time required for each epoch across different experiments and datasets. Training times are reported in seconds for various configurations of the model and datasets.

Table 5
Key 3D ResNet configuration parameters for whole brain and Regions of Interest.

Specification	All brain regions	6 ROIs
Filter Number	128	64
Kernel Size	$7 \times 7 \times 7$	$5 \times 5 \times 5$
ResNet Configuration	[3, 16, 36, 6]	[3, 8, 36, 6]

Table 6
Number of parameters.

Parameter type	All brain regions	6 ROIs
Trainable parameters	264,960,646	59,232,646
Non-trainable parameters	9,984	9,856
Total parameters	264,970,630	59,242,502

Table 4 provides a comparison of training times for different datasets and Regions of Interest (ROIs). The time required varies depending on the dataset and whether all regions or only specific ROIs are used. Generally, the training time is higher for the OASIS dataset compared to the ADNI dataset, reflecting the increased complexity and size of the OASIS dataset. Training times are reduced when only six ROIs are used compared to utilising all brain regions.

When the model processes the entire brain, it requires a larger and more complex network to learn from the various brain structures, resulting in a significantly higher number of parameters [39]. In contrast, when focusing on selected ROIs, the model complexity is reduced, allowing it to operate with fewer parameters while maintaining high accuracy. These regions are smaller and exhibit less variation compared to the whole brain, making the learning process more efficient.

Table 5 outlines the essential configuration parameters of the model for whole brain and ROI-focused experiments.

Table 6 presents the total number of parameters, including both trainable and non-trainable parameters, for models trained on the entire brain versus only selected ROIs. For the whole brain, the model employs 128 filters with a $7 \times 7 \times 7$ kernel size, structured in a ResNet architecture with [3, 16, 36, 6] layers. For the ROI-based configuration, 64 filters with a $5 \times 5 \times 5$ kernel are used, maintaining a similar architecture but reducing the first block's depth to [3, 8, 36, 6]. This adaptation significantly reduces the model complexity while preserving strong predictive performance.

3.3. Comparison with state-of-the-art methods

The accuracy of the proposed model is compared with previous state-of-the-art methods in Alzheimer's Disease research. Table 7 summarises the comparative analysis. The results demonstrate the superior performance and reliability of the proposed model across different experiments and datasets, showing notable advancements over existing methods.

It is important to note that many prior studies did not report detailed analyses of model time complexity. They primarily focused on improving predictive accuracy and model interpretability. Nevertheless, time complexity remains a critical consideration, and addressing it is planned for future work. Working with 3D MRI data naturally entails high computational demands, a common characteristic in this field.

While this study emphasised accuracy improvements, the model complexity aligns with standard practices for handling high-dimensional MRI data. A comparison of accuracy improvements achieved is presented below.

In the "AD vs. CN" classification, the proposed model achieves an accuracy of 88.89% on the ADNI dataset using all brain regions, surpassing the 83.64% accuracy reported by Inan et al. [7] and 85.69% reported by Lei et al. [11]. When focusing on ROIs, the model achieves 93.33%, outperforming Pan et al.'s 90.6% [24] and Yoon et al.'s 91.7% [42].

Table 7
Comparison in terms of accuracy: previous research works vs our research work.

Study	Dataset	AD vs. CN	AD vs. MCI	CN vs. MCI
Inan et al. [7]	ADNI, OASIS	83.64% (ADNI)	91.54% (OASIS)	82.69% (ADNI)
Lei et al. [11]	ADNI-1, ADNI-2, ADNI-3, AIBL, MCAD	85.69%	69.89%	63.34%
Wang et al. [16]	ADNI-1, ADNI-2, ADNI-3	–	92.92% (Conversion from MCI to AD within 4 years)	–
Pan et al. [24]	ADNI, OASIS	90.6%	–	–
ELGeneedy et al. [40]	OASIS	99.68%	–	–
Sang et al. [15]	ADNI	87.50%	–	–
Carcagnìet al. [14]	ADNI, OASIS	75.625%	–	–
Chen et al. [41]	ADNI-1, ADNI-2, ADNI-GO	95.32%	–	–
Yoon et al. [42]	ADNI, AIBL	91.7%	90.1%	89.9%
Saoud et al. [43]	MALPEM-ADNI	90%	74%	84%
Our Model	ADNI (All regions)	**88.89%**	**88%**	**87.27%**
	ADNI (6 ROIs)	**93.33%**	**92%**	**88.2%**
	OASIS (All regions)	**95%**	**98%**	**98.05%**
	OASIS (6 ROIs)	**97.8%**	**98.33%**	**98.6%**

In the "AD vs. MCI" task, the model attains an accuracy of 88% with all brain regions and 92% with ROIs on the ADNI dataset, significantly surpassing Lei et al.'s 69.89% [11]. With the OASIS dataset, accuracies of 98% and 98.33% are achieved for all regions and ROIs, respectively, setting a new benchmark.

For the "CN vs. MCI" classification, the model achieves 87.27% accuracy (all regions) and 88.2% (ROIs) on the ADNI dataset, considerably outperforming prior works. On the OASIS dataset, accuracies reach 98.05% and 98.6%, confirming the robustness and effectiveness of the proposed approach.

3.4. Discussion

The analysis conducted in this study involves two types of preprocessed images: one encompassing all brain regions and another focusing solely on six Regions of Interest (ROIs). For all brain regions, the advantages include detailed visualisations where different brain areas are colour-coded, enhancing understanding and facilitating advanced research. However, the RGB format results in larger image sizes, increasing dataset complexity and imposing higher computational demands. Additionally, the detailed colouring may alter the original greyscale MRI appearance, potentially limiting its utility for certain medical analyses. This increased resource consumption can pose challenges for researchers with limited computational capacity. Fig. 6 shows different views of full brain MRIs.

In contrast, focusing on Regions of Interest (ROIs) provides a more manageable dataset by concentrating on specific brain areas, thus reducing complexity and resource requirements. This targeted approach enhances efficiency for studying particular brain regions pertinent to specific research objectives. Nevertheless, this method may overlook valuable information from other brain areas and could miss unexpected findings revealed through a comprehensive whole-brain analysis. Fig. 7 illustrates different views of brain MRI scans focused on ROIs.

The proposed method enhances ResNet by integrating an ROI-guided approach with a Convolutional Block Attention Module (CBAM), allowing the model to focus on critical regions in 3D MRI scans. This approach improves accuracy and processing speed compared to conventional CNN models. Transformer-based models are powerful but require large datasets and substantial computational resources, posing challenges in the context of medical imaging. Our approach efficiently handles large volumetric datasets, making it more practical for clinical applications.

Graph Convolutional Networks (GCNs) model inter-relationships such as brain connectivity but require additional preprocessing, such as constructing adjacency matrices, which can introduce bias or affect generalisability. The proposed method circumvents these complexities by directly processing MRI images without additional graph construction steps. Federated learning offers promise for data privacy but faces challenges such as handling non-uniform data distributions and communication overheads. While promising, this study prioritises improving model performance on centralised datasets before extending to decentralised approaches.

The model's superior performance on the OASIS dataset compared to ADNI is likely attributed to differences in data quality, distribution, and sample characteristics. OASIS may possess more consistent imaging protocols and cleaner datasets, facilitating better feature extraction, whereas ADNI data may introduce greater variability, impacting generalisation performance.

The ROI-guided approach significantly reduces computational complexity by focusing on the most relevant brain regions. As a result, it increases accuracy and reduces the time required for training and inference. The incorporation of CBAM further boosts performance by enabling the model to attend to critical spatial and channel-wise features, enhancing feature representation and classification accuracy. Together, the integration of CBAM and ROI selection improves model efficiency, achieving higher accuracy while reducing computational costs compared to traditional whole-brain methods.

Saliency maps were generated for both the full brain regions and the Regions of Interest (ROIs) using the ADNI dataset. Fig. 8(a) displays the saliency map for the entire brain region, while Fig. 8(b) shows the saliency map for the ROIs.

By examining these saliency maps, it can be inferred that the selected ROIs are appropriate for application in classification tasks such as Alzheimer's disease detection. The saliency map for the full brain region indicates that the model predominantly focuses on the areas defined as ROIs, validating their relevance. This observation underscores the critical role of Regions of Interest (ROIs) in enhancing the accuracy and interpretability of Alzheimer's disease identification.

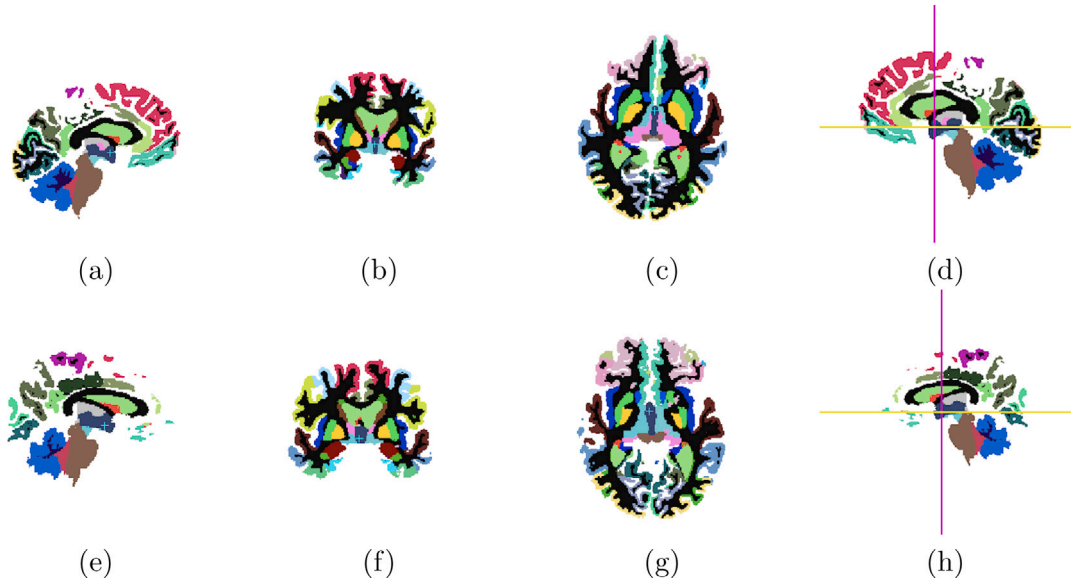


Fig. 6. Instances from ADNI dataset (first row) (a) Sagittal View (b) Coronal View (c) Axial View and (d) Sagittal View with crosshairs pointing to the centre and OASIS dataset (second row).

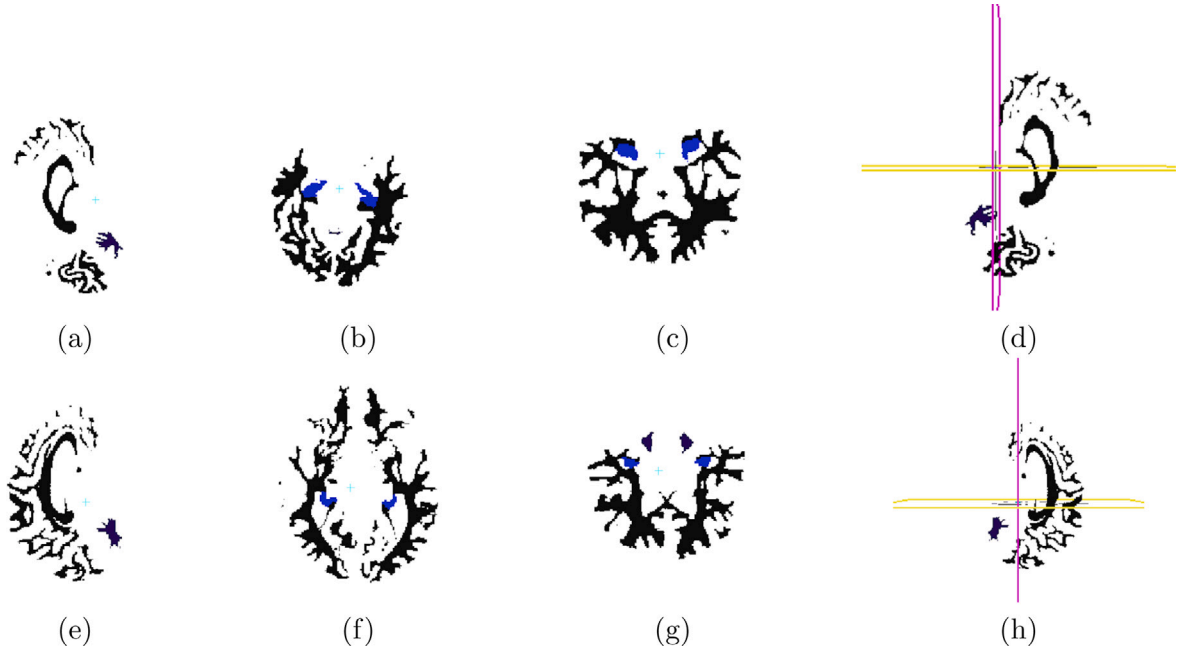


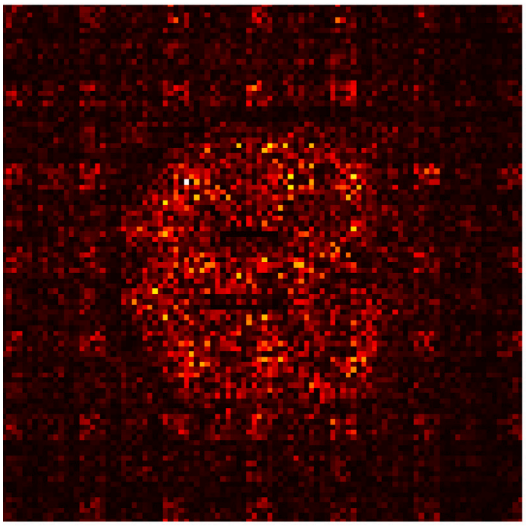
Fig. 7. Preprocessed MRI brain scan using FastSurfer from ADNI dataset (first row) (a) Sagittal View (b) Coronal View (c) Axial View and (d) Sagittal View with crosshairs pointing to the centre and OASIS dataset (second row).

3.5. Future work

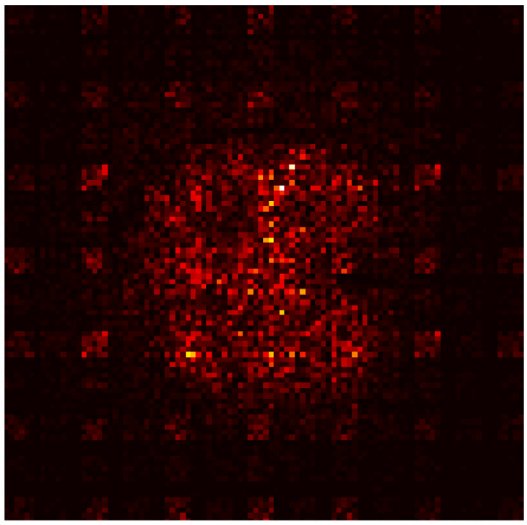
This research will be extended by addressing the current limitations observed with the ADNI dataset. At present, the accuracy for the ADNI dataset ranges from 87.27% to 93.33%, whereas for the OASIS1 dataset, it ranges from 97.8% to 98.6%. To improve performance, specific issues associated with the ADNI dataset will be investigated and resolved. Currently, the analysis focuses on six Regions of Interest (ROIs); however, it is recognised that this may not fully capture the complexity of Alzheimer's-affected brain regions. Thus, future work will include additional ROIs to enhance regional coverage and representation. The updated pipeline will also be validated across additional benchmark datasets to ensure robustness and generalisability. In parallel, a web application is under development that will leverage the proposed pipeline to enable accurate Alzheimer's disease detection from raw 3D MRI inputs, facilitating practical clinical deployment.

4. Conclusion

In this study on Alzheimer's disease detection, a 3D ResNet model was applied to 3D MRI images preprocessed using FastSurfer QuickSeg, employing the ADNI 1.5T and OASIS-1 datasets. MRI data from all brain regions were compared with six specific Regions of Interest (ROIs). Experimental results demonstrated that focusing on six ROIs yielded superior performance: for the ADNI dataset, accuracies improved to 93.33% for AD vs. CN, 92% for AD vs. MCI, and 88.2% for CN vs. MCI. The OASIS dataset exhibited even higher accuracies of 97.8% for AD vs. CN, 98.33% for AD vs. MCI, and 98.6% for CN vs. MCI.



(a) Saliency map of the full brain region.



(b) Saliency map of the Regions of Interest (ROIs).

Fig. 8. Comparison of saliency maps between the full region image (left) and the region of interest (ROI) image (right). The saliency map highlights the most significant areas of the image, where brighter regions indicate higher importance.

This ROI-guided approach not only enhanced detection accuracy but also reduced computational resource requirements, making advanced imaging analysis more accessible and cost-effective. The findings demonstrate the effectiveness of targeted brain region analysis and highlight the potential of integrating AI into medical diagnostics to deliver more precise and efficient healthcare solutions.

CRediT authorship contribution statement

Israt Jahan Khan: Writing – original draft, Visualization, Methodology, Investigation, Data curation, Conceptualization. **Md. Fahim Bin Amin:** Writing – original draft, Visualization, Methodology, Investigation, Data curation, Conceptualization. **Md. Delwar Shahadat Deepu:** Writing – original draft, Visualization, Methodology, Investigation, Data curation, Conceptualization. **Hazera Khatun Hira:** Writing – original draft, Visualization, Methodology, Investigation, Data curation, Conceptualization. **Asif Mahmud:** Writing – original draft, Visualization, Methodology, Investigation, Data curation, Conceptualization. **Anas Mashad Chowdhury:** Writing – original draft, Visualization, Data curation. **Salekul Islam:** Writing – original draft, Visualization, Validation. **Md. Saddam Hossain Mukta:** Writing – original draft, Visualization, Validation. **Swakkhar Shatabda:** Writing – review & editing, Writing – original draft, Visualization, Validation, Supervision, Methodology, Investigation, Formal analysis, Data curation, Conceptualization.

Ethical statement

This study was conducted in accordance with the highest ethical standards and the principles outlined in the Declaration of Helsinki. No human participants, personal data, or identifiable human images were used in this research. Therefore, ethical approval and informed consent were not required.

Declaration of Generative AI and AI-assisted technologies in the writing process

During the preparation of this work, ChatGPT-4.0 was used to improve language and readability. After using this tool, the authors reviewed and edited the content as needed and took full responsibility for the content of the publication.

Declaration of competing interest

The authors declare that they have no known competing financial interests or personal relationships that could have appeared to influence the work reported in this paper.

References

[1] Balasundaram A, Srinivasan Sruthi, Prasad A, Malik Jahan, Kumar Ayush. Hippocampus segmentation-based alzheimer's disease diagnosis and classification of mri images. Arab J Sci Eng 2023;1–17.
[2] Scheltens Philip, Strooper Bart De, Kivipelto Miia, Holstege Henne, Chételat Gael, Teunissen Charlotte E, et al. Alzheimer's disease. Lancet 2021;397(10284):1577–90.
[3] Zhao Xinxing, Ang Candice Ke En, Acharya U Rajendra, Cheong Kang Hao. Application of artificial intelligence techniques for the detection of alzheimer's disease using structural mri images. Biocybern Biomed Eng 2021;41(2):456–73.
[4] Pini Lorenzo, Pievani Michela, Bocchetta Martina, Altomare Daniele, Bosco Paolo, et al. Brain atrophy in alzheimer's disease and aging. Ageing Res Rev 2016;30:25–48.
[5] Helaly Hadeer A, Badawy Mahmoud, Haikal Amira Y. Deep learning approach for early detection of alzheimer's disease. Cogn Comput 2022;14(5):1711–27.
[6] Zhang Shuo, Liu Zhiwen, Chen Yunping, Jin Yulin, Bai Guosheng. Selective kernel convolution deep residual network based on channel-spatial attention mechanism and feature fusion for mechanical fault diagnosis. ISA Trans 2023;133:369–83.
[7] Inan Muhammad Sakib Khan, Sworna Nabila Sabrin, Islam AKM Muzahidul, Islam Salekul, Alom Zulfikar, Azim Mohammad Abdul, et al. A slice selection guided deep integrated pipeline for alzheimer's prediction from structural brain mri. Biomed Signal Process Control 2024;89:105773.
[8] Arya Akhilesh Deep, Verma Sourabh Singh, Chakarabarti Prasun, Chakrabarti Tulika, Elngar Ahmed A, Kamali Ali-Mohammad, et al. A systematic review on machine learning and deep learning techniques in the effective diagnosis of alzheimer's disease. Brain Informatics 2023;10(1):17.
[9] Biswas Rashni, J. Rolant Gini. Multi-class classification of alzheimer's disease detection from 3d mri image using ml techniques and its performance analysis. Multimedia Tools Appl 2024;83(11):33527–54.
[10] Ayus Ishan, Gupta Deepak. A novel hybrid ensemble based alzheimer's identification system using deep learning technique. Biomed Signal Process Control 2024;92:106079.
[11] Lei Baiying, Liang Yu, Xie Jiayi, Wu You, Liang Enmin, Liu Yong, et al. Hybrid federated learning with brain-region attention network for multi-center alzheimer's disease detection. Pattern Recognit 2024;153:110423.
[12] El-Assy AM, Amer Hanan M, Ibrahim HM, Mohamed MA. A novel cnn architecture for accurate early detection and classification of alzheimer's disease using mri data. Sci Rep 2024;14(1):3463.
[13] Helaly Hadeer A, Badawy Mahmoud, Haikal Amira Y. Toward deep mri segmentation for alzheimer's disease detection. Neural Comput Appl 2022;34(2):1047–63.

[14] Carcagnì Pierluigi, Leo Marco, Coco Marco Del, Distante Cosimo, Salve Andrea De. Convolution neural networks and self-attention learners for alzheimer dementia diagnosis from brain mri. Sensors 2023;23(3):1694.
[15] Sang Yilin, Li Wan. Classification study of alzheimer's disease based on self-attention mechanism and dti imaging using gcn. IEEE Access 2024.
[16] Wang Yifan, Gao Ruitian, Wei Ting, Johnston Luke, Yuan Xin, Yue Zhang others. Predicting long-term progression of alzheimer's disease using a multimodal deep learning model incorporating interaction effects. J Transl Med 2024;22(1):265.
[17] Yaqoob Nabeela, Khan Muhammad Attique, Masood Saleha, Albarakati Hussain Mobarak, Hamza Ameer, Alhayan Fatimah, Jamel Leila, Masood Anum. Prediction of Alzheimer's disease stages based on ResNet-Self-attention architecture with Bayesian optimization and best features selection. Frontiers in Computational Neuroscience 2024;18. 1393849.
[18] Gamal Aya, Elattar Mustafa, Selim Sahar. Automatic Early Diagnosis of Alzheimer's Disease Using 3D Deep Ensemble Approach. IEEE Access 2022;10:115974–87.
[19] Diogo Vasco Sá, Ferreira Hugo Alexandre, Prata Diana, Alzheimer's Disease Neuroimaging Initiative. Early diagnosis of alzheimer's disease using machine learning: a multi-diagnostic, generalizable approach. Alzheimer' s Res Ther 2022;14(1):107.
[20] He Baiqing. Research on multi-modal medical image fusion based on multi-scale attention mechanism. J Phys: Conf Ser 2022;2173:012037.
[21] Galety Mohammad Gouse, Gupta Shweta. Artificial intelligence in the detection of alzheimer's disease. In: Bio-inspired algorithms and devices for treatment of cognitive diseases using future technologies. IGI Global; 2022, p. 136–55.
[22] Shukla Gargi Pant, Kumar Santosh, Pandey Saroj Kumar, Agarwal Rohit, Varshney Neeraj, Kumar Ankit. Diagnosis and detection of alzheimer's disease using learning algorithm. Big Data Min Anal 2023;6(4):504–12.
[23] Klingenberg Malte, Stark Didem, Eitel Fabian, Budding Céline, Habes Mohamad, Ritter Kerstin, et al. Higher performance for women than men in mri-based alzheimer's disease detection. Alzheimer' s Res Ther 2023;15(1):84.
[24] Pan Dan, Zeng An, Yang Baoyao, Lai Gangyong, Hu Bing, Song Xiaowei, et al. Deep learning for brain mri confirms patterned pathological progression in alzheimer's disease. Adv Sci 2023;10(6):2204717.
[25] Shamrat FM Javed Mehedi, Akter Shamima, Azam Sami, Karim Asif, Ghosh Pronab, Tasnim Zarrin, et al. Alzheimernet: An effective deep learning based proposition for alzheimer's disease stages classification from functional brain changes in magnetic resonance images. IEEE Access 2023;11:16376–95.
[26] Rangaraju Banupriya, Chinnadurai Thilagavathi, Natarajan Sarmiladevi, Raja Vishnu. Dual attention aware octave convolution network for early-stage alzheimer's disease detection. Inf Technol Control 2024;53(1):302–16.
[27] Ramya J, Maheswari B Uma, Rajakumar MP, Sonia R. Alzheimer's disease segmentation and classification on mri brain images using enhanced expectation maximization adaptive histogram (eem-ah) and machine learning. Inf Technol Control 2022;51(4):786–800.
[28] Odusami Modupe, Maskeliūnas Rytis, Damaševičius Robertas, Misra Sanjay. Explainable deep-learning-based diagnosis of alzheimer's disease using multimodal input fusion of pet and mri images. J Med Biological Eng 2023;43(3):291–302.
[29] Odusami Modupe, Damaševičius Robertas, Milieškaitė-Belousovienė Egle, Maskeli Rytis. Alzheimer's disease stage recognition from mri and pet imaging data using pareto-optimal quantum dynamic optimization. Heliyon 2024;10(15).
[30] Yaqoob Nabeela, Khan Muhammad Attique, Masood Saleha, Albarakati Hussain Mobarak, Hamza Ameer, Alhayan Fatimah, et al. Prediction of alzheimer's disease stages based on resnet-self-attention architecture with bayesian optimization and best features selection. Front Comput Neurosci 2024;18:1393849.
[31] Shankar KC Prabu, Shyry S Prayla. Medical image segmentation using hybrid contrast limited adaptive histogram equalization (clahe) and expectation maximization algorithm. J Intell Fuzzy Systems 1–16, (Preprint).
[32] Woo Sanghyun, Park Jongchan, Lee Joon-Young, Kweon In So. Cbam: Convolutional block attention module. In: Proceedings of the European conference on computer vision. 2018, p. 3–19.
[33] Ouyang Daliang, He Su, Zhang Guozhong, Luo Mingzhu, Guo Huaiyong, Zhan Jian, et al. Efficient multi-scale attention module with cross-spatial learning. In: ICASSP 2023-2023 IEEE international conference on acoustics, speech and signal processing. IEEE; 2023, p. 1–5.
[34] Saratxaga Cristina L, Moya Iratxe, Picón Artzai, Acosta Marina, Moreno-Fernandez-de Leceta Aitor, Garrote Estibaliz, et al. Mri deep learning-based solution for alzheimer's disease prediction. J Pers Med 2021;11(9):902.
[35] Henschel Leonie, Conjeti Sailesh, Estrada Santiago, Diers Kersten, Fischl Bruce, Reuter Martin. Fastsurfer-a fast and accurate deep learning based neuroimaging pipeline. NeuroImage 2020;219:117012.
[36] Brickman Adam M, Buchsbaum Mindy S, Blacker Deborah, Tang Ming-X, Stern Yaakov. Measuring cerebral atrophy and white matter hyperintensity burden to predict the rate of cognitive decline in alzheimer disease. Arch Neurol 2008;65(3):394–8.
[37] Kalyani Jagriti, Chakraborty Monisha. Contrast enhancement of mri images using histogram equalization techniques. In: 2020 international conference on computer, electrical & communication engineering. 2020, p. 1–5.
[38] der Walt Stefan Van, Schönberger Johannes L, Nunez-Iglesias Juan, Boulogne François, Warner Joshua D, Yager Neil, et al. Scikit-image: image processing in python. PeerJ 2014;2:e453.
[39] Reeja J Jackulin, Arun CH. Three-and two-dimensional deep neural network for acute ischemic stroke identification in t1-weighted magnetic resonance imaging. Multimedia Tools Appl 2024;1–19.
[40] EL-Geneedy Marwa, Moustafa Hossam El-Din, Khalifa Fahmi, Khater Hatem, AbdElhalim Eman. An mri-based deep learning approach for accurate detection of alzheimer's disease. Alex Eng J 2023;63:211–21.
[41] Chen Yuanyuan, Xia Yong. Iterative sparse and deep learning for accurate diagnosis of alzheimer's disease. Pattern Recognit 2021;116:107944.
[42] Yoon Dan, Myong Youho, Kim Young Gyun, Sim Yongsik, Cho Minwoo, Oh Byung-Mo, et al. Latent diffusion model-based mri superresolution enhances mild cognitive impairment prognostication and alzheimer's disease classification. NeuroImage 2024;120663.
[43] Saoud Lyes Saad, AlMarzouqi Hasan. Explainable early detection of alzheimer's disease using rois and an ensemble of 138 3d vision transformers. Sci Rep 2024;14(1):27756.